Preparation and thermal performance regulation of multidimensional carbon-based microencapsulated phase change composites*

HE Chenbo[1], WANG Zihan[1], TANG Guihua[1], SUN Jingjing[2], SUN Chencheng[2], LI Junning[2], WANG Xiaoyan[2]

1. MOE Key Laboratory of Thermo-Fluid Science and Engineering, School of Energy and Power Engineering, Xi'an Jiaotong University, Xi'an 710049, China

2. Science and Technology on Advance Functional Composites Laboratory, Aerospace Research Institute of Materials & Processing Technology, Beijing 100076, China

Abstract

To meet the requirements of spacecraft thermal management materials for both high thermal conductivity and large latent heat storage capacity, a multidimensional carbon-based microencapsulated phase change composite with enhanced thermal performance was prepared using a hot-pressing technique. This method addresses two major limitations of conventional phase change materials: low thermal conductivity and susceptibility to liquid leakage. The effects of content and ratios of microencapsulated phase change materials, flake graphite, and pitch-based carbon fibers on thermal conductivity and latent heat were systematically studied through a combination of experiments and finite element simulations. Furthermore, the formation mechanism of the internal multidimensional thermal conduction network was clarified. Results showed that introducing multidimensional thermally conductive fillers into the microencapsulated phase change system and optimizing the component composition and structure can effectively establish a continuous and dense carbon-based thermal conduction network. Leveraging the synergy between these conductive fillers and a multi-size flake graphite filling strategy, the composite achieved a significantly improved thermal conductivity of 1.021 W/(m·K) while maintaining a high latent heat of 81.540 J/g. These findings provide theoretical and practical guidance for developing advanced thermal management materials for spacecrafts.

Keywords: spacecraft thermal management, microcapsule phase change composite material, multidimensional carbon-based network, synergistic thermal enhancement

PACS: 44.05.+e, 44.10.+i, 05.70.Fh, 81.20.–n

---

* The paper is an English translated version of the original Chinese paper published in Acta Physica Sinica. Please cite the paper as: HE Chenbo, WANG Zihan, TANG Guihua, SUN Jingjing, SUN Chencheng, LI Junning, WANG Xiaoyan. Preparation and thermal performance tuning of multidimensional carbon-based microcapsule phase change composites, Acta Phys. Sin., 2025, 74(7): 074401. doi: 10.7498/aps.74.20241731

1. Introduction

In high-precision missions such as space gravitational wave detection, slight thermal fluctuations within the spacecraft can significantly affect gravitational wave measurements, thereby reducing the reliability of detection results [1,2]. Paraffin, as a traditional thermal management phase change material (PCM), exhibits high latent heat and chemical stability [3]. It can effectively store and release heat through solid-liquid phase change, thus maintaining thermal stability within spacecraft. Wu et al. proposed a spacecraft thermal control system based on shape-stable phase change materials [4] and demonstrated that these materials could effectively prevent system failure under dramatic external heat flux changes. However, paraffin still faces two major challenges in practical applications: (1) Liquid leakage. Paraffin tends to leak above its melting temperature, reducing its heat storage capacity and cycle stability [5]. (2) Low thermal conductivity. Paraffin's thermal conductivity is approximately 0.2 W/(m·K) [6], which limits efficient internal heat transfer, making it difficult to rapidly absorb power fluctuations within spacecraft.

To address the leakage issue, current research primarily focuses on encapsulating phase change materials into microcapsule (PCMC) with core-shell structures using polymers [7–9]. Encapsulating paraffin ensures that its solid-liquid transitions occur within the microcapsules, effectively preventing leakage and improving cycle stability. Wang et al. [10] prepared paraffin@methyl methacrylate/silica hybrid-shell microcapsules via interfacial hydrolysis-polycondensation, achieving energy storage efficiency exceeding 99.9%. Zhang et al. [11] synthesized paraffin@silica core-shell microcapsules through a sol-gel method combined with silane coupling agent modification, achieving an encapsulation efficiency of 99.9 % for latent- heat storage and restricting paraffin leakage to only 1.24 %.

However, the high interfacial thermal resistance of PCMC significantly reduces the melting and solidification rates of encapsulated paraffin. Two main strategies have been proposed to address this: (1) introducing thermally conductive additives to enhance the overall thermal conductivity of PCMC composites; and (2) embedding PCMC into high thermal conductivity matrices to accelerate thermal response [12,13]. Carbon-based thermal conductivity enhancers offer advantages including high thermal conductivity, low density, high specific surface area, and good chemical stability, along with diverse morphology and sizes. Among these, pitch-based carbon fibers (PCFs) and flake graphite (FG) have gained significant attention due to their excellent thermal conductivity and unique structural characteristics [14]. As a one-dimensional material, PCF exhibits axial thermal conductivity greater than 900 W/(m·K) along with high mechanical strength, thereby enhancing both thermal and mechanical properties of phase change composites [15]. FG possesses a two-dimensional layered structure with an in-plane thermal conductivity exceeding 500 W/(m·K) and a large specific surface area (~2 m^2/g), allowing efficient thermal contact with

the PCM [16]. Xia et al. [17] prepared a three-dimensional layered phase change composite using graphene oxide, significantly enhancing thermal conductivity to 0.48 W/(m·K) and latent heat to 158.2 J/g. Nomura et al. [18] fabricated erythritol@carbon fiber phase change composites using hot pressing, demonstrating that hot pressing effectively promotes the formation of thermal conduction networks, significantly improving thermal conductivity even with low filler concentrations.

Although previous studies have alleviated issues of liquid leakage and low thermal conductivity, research has mostly focused on using a single type of thermal conductivity enhancer. A thermal conduction network composed of a single material type often lacks sufficient compactness and connectivity, making it difficult to establish efficient thermal conduction pathways and thus limiting the thermal response rate [19,20]. Moreover, the synergistic effect mechanisms of multidimensional thermal conductivity enhancers in phase change composites remain unclear. Therefore, in this work, multidimensional carbon-based thermal conductivity enhancers (FG and PCF) were introduced, and a multidimensional carbon-based microencapsulated phase change composite with high thermal conductivity and high latent heat was prepared by a hot-pressing method. The influences of the content and ratio of PCMC (zero-dimensional), PCF (one-dimensional), and FG (two-dimensional) with different sizes on the composite's thermal conductivity and latent heat were investigated experimentally. Additionally, the heat transfer mechanism of the multidimensional carbon-based thermal conduction network was elucidated via finite element simulation.

2. Methods

2.1 Experimental material

The PCMC consists of n-heptadecane as the core material and polymethyl methacrylate as the shell material. The average particle size of PCMC is 5 μm, provided by Hefei Xinneng Phase Change New Material Technology Co., Ltd. Flake graphite (FG), supplied by Forsman Technology (Beijing) Co., Ltd., has diameters of 10, 50, and 100 μm, a thickness of 2 μm, a density of 2.26 g/cm^3, exhibits thermal conductivities of 523 W/(m·K) in the in-plane direction and 38 W/(m·K) in the out-of-plane direction, respectively. Pitch-based carbon fiber (PCF), also from Forsman Technology (Beijing) Co., Ltd., has a diameter of 10 μm, a length of 25 mm, a density of 2.23 g/cm^3, and axial and radial thermal conductivities of 960 and 10 W/(m·K), respectively [22]. Anhydrous ethanol (analytically pure) was purchased from Shanghai Titan Technology Co., Ltd.

2.2 Sample preparation

In this paper, the hot-pressing process was employed to promote interfacial bonding and densification of the constituent materials under specific temperature and pressure, preparing multidimensional carbon-based microencapsulated phase-change composites with enhanced

thermal conductivity. Fig. 1 shows the preparation flowchart. The detailed preparation steps are as follows:

1) Proportioning and weighing. A total of 15 groups of samples were prepared, and the mass fractions of each component material are listed in Table 1. Samples 1-9 were designed using orthogonal experimental methods to optimize FG mixing ratios of different sizes; Samples 10-12 were control groups for samples 1-9, containing only single-sized FG; Samples 13 and 14 served as control groups for Sample 5, with PCMC mass fractions of 80% and 90%, respectively; Sample 15, another control group for Sample 5, contained only FG and PCMC without PCF.

Table 1. Mass fractions of each component in the phase change composites.

Sample	10μm FG /%	50μm FG /%	100μm FG /%	PCMC /%	PCF /%
1	4.25	4.25	16.50	70.00	5.00
2	4.25	8.25	12.50	70.00	5.00
3	4.25	12.50	8.25	70.00	5.00
4	8.25	4.25	12.50	70.00	5.00
5	8.25	8.25	8.50	70.00	5.00
6	8.25	12.50	4.25	70.00	5.00
7	12.50	4.25	8.25	70.00	5.00
8	12.50	8.25	4.25	70.00	5.00
9	12.50	12.50	0.00	70.00	5.00
10	25.00	0.00	0.00	70.00	5.00
11	0.00	25.00	0.00	70.00	5.00
12	0.00	0.00	25.00	70.00	5.00
13	4.95	4.95	5.10	80.00	5.00
14	1.65	1.65	1.70	90.00	5.00
15	9.90	9.90	10.20	70.00	0.00

2) Stirring and dispersion. PCMC was mixed with 500 mL absolute ethanol and mechanically stirred at 800-1000 rpm for 20 min to form a homogeneous suspension. Then FG and PCF were slowly added, and stirring continued until all components were uniformly dispersed.

3) Drying. The mixed suspension was transferred into an electric blast drying oven and dried at 80 ℃ for 12 h to completely volatilize the ethanol and yield a uniform powder mixture. During drying, the samples were periodically shaken to prevent agglomeration and improve drying efficiency.

4) Hot-pressing. The dried powder mixture was placed into a mold, hot-pressed at 100 ℃ under 20 MPa pressure for 6 h, and the pressure was maintained for an additional 4 h while cooling slowly to room temperature. The entire hot-pressing process was performed in a nitrogen environment to prevent oxidation.

5) Demolding and trimming. After demolding, cylindrical samples measuring 5 cm in diameter and 2 cm in thickness with a density of 1 g/cm^3 were obtained. The samples were machined to remove surface burrs to meet testing requirements.

Figure 1. Flowchart of the preparation process for multidimensional carbon-based thermally enhanced microcapsule phase change composite.

2.3 Performance characterization

The morphology of the multidimensional carbon-based microencapsulated phase-change composites was observed using a Zeiss Sigma 300 scanning electron microscope (SEM). Samples were fixed on the stage with conductive adhesive, platinum-coated for 90 s, and tested at voltages ranging from 3-15 kV. The thermal conductivity was measured using a TPS2500S thermal constant analyzer (HotDisk, Sweden) based on the transient plane heat source method, employing a 5465-polyimide probe. The tested composite samples were cylindrical with a diameter of 5 cm and thickness of 2 cm. Latent heat and phase-transition temperatures were determined by a NETZSCH 3500 Sirius differential scanning calorimeter (DSC) from -20 to 100 ℃ at a heating/cooling rate of 5 ℃/min in nitrogen. Thermal cycling tests were performed using a BPS-100CA constant temperature and humidity chamber (Shanghai Precision Instrument Co., Ltd.). Samples were heated from room temperature (25 ℃) to 80 ℃ for 10 min, then cooled to -10 ℃ for another 10 min, up to 100 cycles.

2.4 Numerical model

The random sequential adsorption (RSA) method was used to numerically reconstruct the representative volume element (RVE) model of the phase-change composite, as illustrated in Fig. 2. The heat conduction process of the composite was simulated using finite element analysis. To simplify the numerical model, the following assumptions were made: 1) FG flakes have a regular hexagonal structure; 2) PCMCs are embedded within a

multidimensional carbon-based conductive network, assuming perfect interfacial bonding; 3) The PCMC-filled matrix is treated as a homogeneous material. The specific steps are as follows.

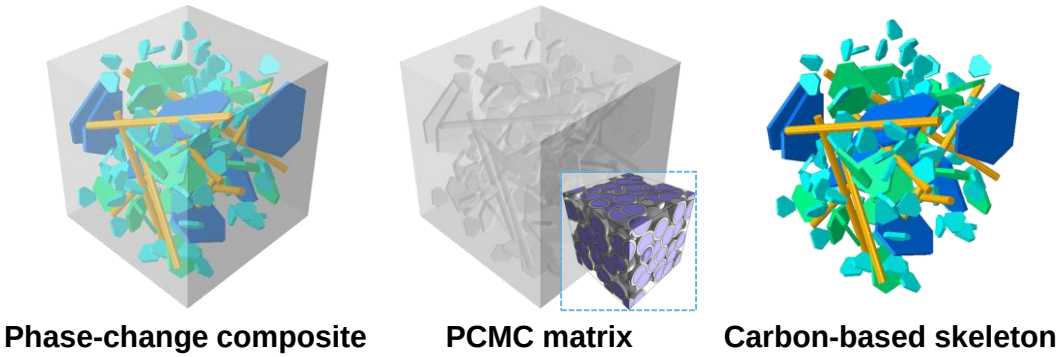

Figure 2. Schematic diagram of the RVE model for multidimensional carbon-based thermally enhanced microcapsule phase change composite.

1) FG and PCF were randomly distributed using the RSA method according to their structural parameters described in Section 2.1, numerically reconstructing the RVE model [20].

2) Periodic temperature boundary conditions [23] were applied to the front, back, left, and right faces of the RVE model, ensuring continuity of temperature and heat flux at boundary nodes through multi-point constraints:

$$T^{+} - T^{-} = T^{*} \tag{1}$$

Where T^{+} and T^{-} represent temperatures at periodic node sets on opposite parallel boundaries, and T^{*} is the periodic temperature correction.

3) Constant temperature boundary conditions were imposed at the top (300 K, hot side) and bottom (273 K, cold side) to establish unidirectional heat conduction.

4) The heat flux at integration points within the RVE was calculated by finite element analysis. The average heat flux was determined based on numerical homogenization theory [23]:

$$\langle q \rangle_i = \frac{1}{V_{RVE}} \sum_{I=1}^{n_{\text{int}}} q_i(x_I) \cdot IVOL(x_1) \tag{2}$$

Where $\langle q \rangle_i$ is the average heat flux, q_i is the heat flux at each integration point, IVOL is the integration point volume, and V_{RVE} is the total RVE volume.

5) Using the average heat flux and temperature gradient, the equivalent thermal

conductivity was calculated by using Fourier law.

6) The Automatic method of ABAQUS is used to discretize the RVE model. The RVE dimensions were 2.5×10^{-4} m, and the mesh size is 2×10^{-6} m. A 10- node quadratic tetrahedral heat- transfer element (DC3D10) was employed.

2.5 Calculation of Thermal Conductivity of PCMC Filled Matrix

To determine basic thermophysical parameters of the homogeneous matrix, thermal conductivities of single PCMC and PCMC-filled matrix were calculated by the Maxwell–Eucken and Bruggeman models, respectively. The PCMC has a core-shell structure, and its equivalent thermal conductivity was calculated using the Maxwell–Eucken model [24,25]:

$$\lambda_{\text{eff}}^{\text{PCMC}} = \lambda_{\text{core}}\left(\frac{\lambda_{\text{shell}} + 2\lambda_{\text{core}} + 2f_{\text{core}}(\lambda_{\text{shell}} - \lambda_{\text{core}})}{\lambda_{\text{shell}} + 2\lambda_{\text{core}} - f_{\text{core}}(\lambda_{\text{shell}} - \lambda_{\text{core}})}\right) \quad (3)$$

Where $\lambda_{\text{eff}}^{\text{PCMC}}$ is the equivalent thermal conductivity of the PCMC; λ_{core} (n-heptadecane core) is 0.197 W/(m K) [6]; λ_{shell} (poly methyl methacrylate shell) is 0.21 W/(m K) [26]; and f_{core} is the volume fraction of the core material, calculated by

$$f_{\text{core}} = \left(\frac{d_{\text{core}}}{d_{\text{total}}}\right)^3 \quad (4)$$

Where d_{core} is the core diameter of PCMC, which is 4.5 μm; The d_{total} is the total particle size of PCMC. The equivalent thermal conductivity of a single PCMC was calculated as 0.198 W/(m K). In the RVE model of multi-dimensional carbon-based microencapsulated phase change composites, the homogeneous matrix is regarded as the close-packed structure of PCMC, and when the PCMC is rhombohedral, it forms a cubic close-packed structure, and its porosity is calculated by [27].

$$\varphi = 1 - \left(\frac{2\pi}{6\sqrt{2}}\right) \quad (5)$$

Where φ is the porosity of the matrix, and the calculated φ is 25.95%. For the PCMC filled matrix with micropores, the equivalent thermal conductivity can be calculated by Bruggeman model [27,28]:

$$\varphi\left(\frac{\lambda_{\text{air}} - \lambda_{\text{matrix}}}{\lambda_{\text{air}} + 2\lambda_{\text{matrix}}}\right) + (1-\varphi)\left(\frac{\lambda_{\text{PCMC}} - \lambda_{\text{matrix}}}{\lambda_{\text{PCMC}} + 2\lambda_{\text{matrix}}}\right) = 0 \quad (6)$$

Where λ_{air} is the thermal conductivity of air (at room temperature), and the value is 0.026

W/(m ·K); the thermal conductivity of PCMC-filled matrix λ_{matrix}, was obtained by an iterative numerical solution as 0.156 W/(m ·K).

3. Results and Discussion

3.1 Micromorphology

The morphology of the multidimensional carbon-based microencapsulated phase change composite (Sample 5) is shown in Fig. 3. In Fig. 3(a), the PCMC particles display irregular spherical shapes with intact polymethyl methacrylate shells, indicating effective encapsulation, which prevents leakage of PCM and enhances durability. In Figs. 3(b) and 3(c), two-dimensional flake graphite (FG) and one-dimensional pitch-based carbon fibers (PCF) are densely packed by the hot-pressing process, collaboratively forming a multidimensional carbon-based thermal conduction network. Additionally, zero-dimensional spherical PCMCs uniformly adhere to the surfaces of FG and PCF, ensuring strong interfacial bonding, reducing interfacial thermal resistance, and promoting an efficient heat conduction pathway.

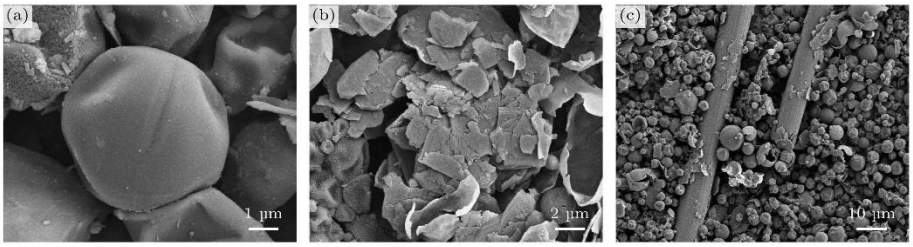

Figure 3. Scanning electron microscopy images of multidimensional carbon-based thermally enhanced microencapsulated phase change composites: (a) PCMC; (b) FG skeleton structure; (c) PCF-doped composite.

3.2 Effect of PCMC content on thermophysical properties of phase change composites

Figure 4 shows the DSC curves of multidimensional carbon-based microencapsulated phase change composites containing 70% (Sample 5), 80% (Sample 13), and 90% (Sample 14) PCMC. The shapes of the phase transition peaks for the three samples are similar, exhibiting multiple transitions corresponding to the solid–solid phase transition (monoclinic to hexagonal) and solid–liquid transition of n-heptadecane. Moreover, the phase transition temperatures of the samples remain essentially unchanged, with the endothermic and exothermic transition temperatures at approximately 14.9 °C and 21.1 °C, respectively.

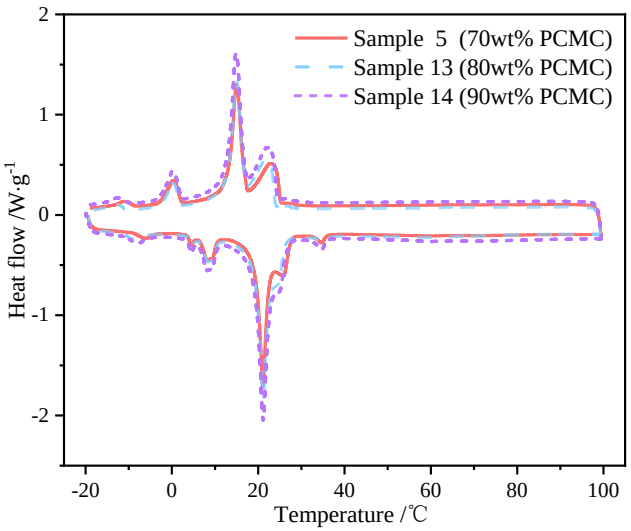

Figure 4. DSC curves of phase change composites with different PCMC contents.

Fig. 5 presents the thermal conductivity (λ) and latent heat (ΔH) results of phase change composites with varying PCMC contents. Sample 14 (90% PCMC) exhibits the highest ΔH, confirming that increased PCMC content improves heat storage capability. However, the λ of Sample 14 is only 0.591 W/(m K) due to the intrinsically low thermal conductivity of PCMC, restricting efficient heat transfer paths. Conversely, Sample 5 (70% PCMC) achieves a high λ of 0.887 W/(m K) because lower PCMC content allows FG and PCF to form a continuous multidimensional thermal conduction network, significantly enhancing the composite's thermal response rate.

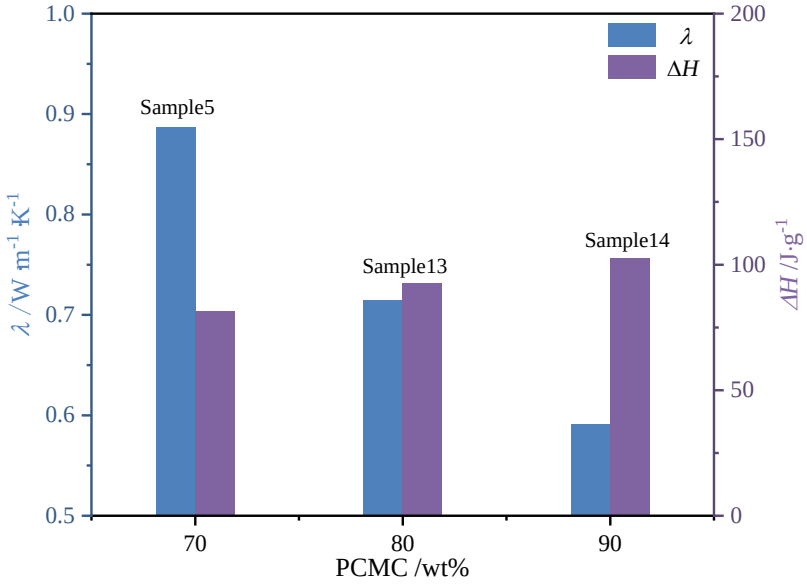

Figure 5. Thermal performance of phase change composites with different PCMC contents.

To achieve the optimal balance between thermal conductivity and latent heat, comparative analysis indicates that Sample 5 (70% PCMC), with ΔH of 81.282 J/g (only

20.6% lower than Sample 14) and λ increased by 50.1%, exhibits excellent thermal management performance. Therefore, 70% PCMC was selected as the optimal composition for subsequent experiments.

3.3 Effect of PCF on Thermophysical Properties of Phase Change Composites

To investigate the effect of PCF on thermophysical properties, phase change composites with and without PCF were evaluated (Table 2). Sample 5 (doped with 5% PCF) is significantly higher than that of Sample 15 (without doping PCF) by 153.4%. This demonstrates that synergistically doping multidimensional conductive materials substantially enhances thermal conductivity by constructing efficient thermal conduction networks. Meanwhile, the ΔH of Sample 5 (81.282 J/g) remains similar to Sample 15 (80.241 J/g), indicating that adding PCF does not compromise the latent heat capacity.

Table 2. Comparison of thermal performance between PCF-containing and PCF-free composites.

Sample	PCF /wt%	λ /W m^{-1} K^{-1}	ΔH /J g^{-1}
5	5	0.887	81.282
15	0	0.350	80.241

To further clarify the enhancement mechanism of PCF on the thermal conductivity of phase change composites, RVEs of multidimensional carbon-based microencapsulated phase change composites with and without PCF were constructed, and finite element simulations of thermal conduction were carried out. Figs. 6(a, b) present the temperature gradient distributions of the RVE models. As illustrated in Fig. 6(c), PCF forms one-dimensional thermal conduction pathways within the composite. These pathways interconnect with the two-dimensional thermal conduction channels provided by FG, collaboratively constructing a multidimensional carbon-based thermal conduction network. Additionally, the one-dimensional PCF effectively fills gaps between FG layers, increasing the contact area between thermally conductive materials and the PCMC matrix, thus enhancing internal heat-transfer connectivity and stability. In contrast, as shown in Fig. 6(d), the thermal conduction paths in the composite without PCF primarily rely on two-dimensional planar conduction via FG sheets. Although this planar network enables basic heat transfer, the discontinuity of thermal paths significantly reduces the thermal response rate. Therefore, introducing multidimensional thermally conductive materials effectively creates synergistic enhancement effects, significantly shortens the heat transfer pathways, improves thermal response characteristics, and provides robust support for thermal management during heat absorption and release processes.

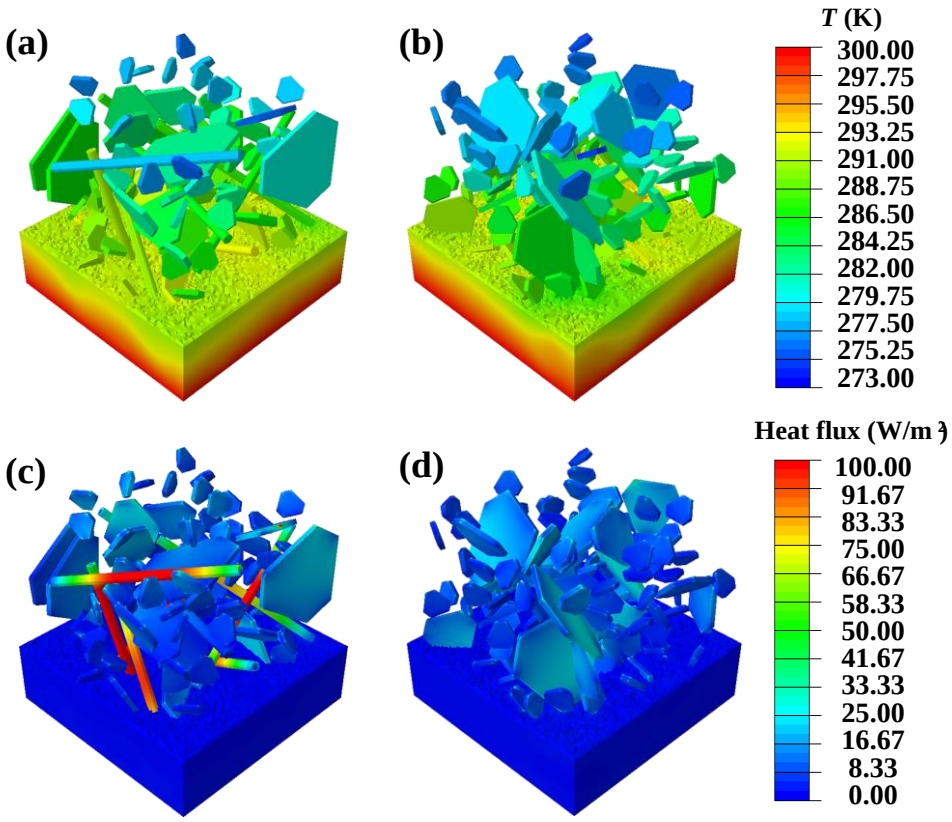

Figure 6. Finite element analysis of thermal conduction: (a) Temperature distribution with PCF; (b) without PCF; (c) heat flux distribution with PCF; (d) without PCF.

3.4 Effect of FG Mixing Ratio on Thermophysical Properties of Phase Change Composites

To explore the influence of FG size (10,50 and 100 μm) on the thermophysical properties of composites, the orthogonal experimental design of three factors and three levels was adopted in Sample 1-9. Three FG sizes were used as experimental factors, and each factor was set at three levels of low, medium and high, thus forming nine experimental combinations, which helps reveal the effect of FG mixing ratio on the thermal properties of multi-dimensional carbon-based thermal conductivity enhanced microencapsulated phase change composites, and can also avoid too large experimental combinations. As a control, Sample 10-12 only uses a single size of FG, and the specific proportion of FG in each sample is shown in Fig. 7.

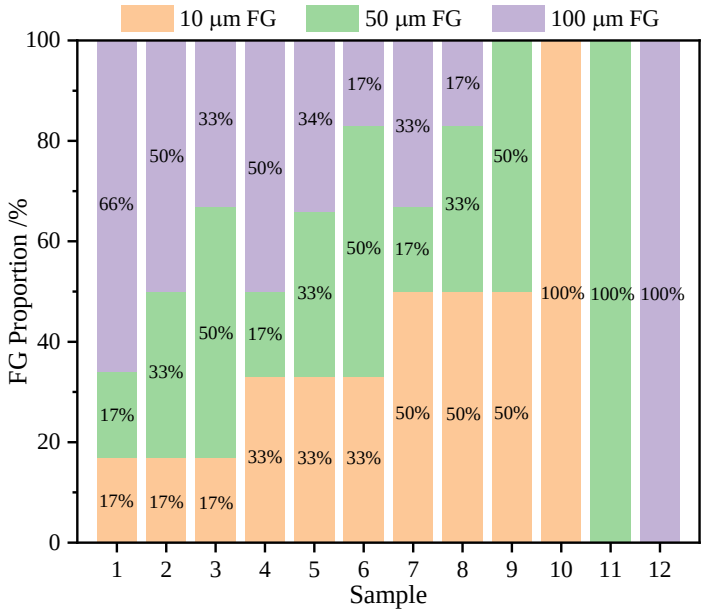

Figure 7. Mixing ratios of FG with different sizes in Samples 1–12.

The experimental results for λ and ΔH of Samples 1-12 are shown in Fig. 8. Among these samples, Sample 8, containing 50% FG (10 μm), 33% FG (50 μm), and 17% FG (100 μm), exhibited the highest λ value of 1.021 W/(m K). This thermal conductivity was significantly higher than that of Samples 10-12, which contained single-size FG (0.923, 0.835, and 0.672 W/(m K), respectively). Meanwhile, the ΔH values of Samples 1-12 were approximately equivalent, with Sample 8 showing a latent heat of 81.54 J/g. These results indicate that filling the composite with multi-scale FG significantly enhances its thermal conductivity without compromising latent heat storage performance. Single-scale FG networks exhibit limited connectivity and compactness due to their structural constraints. Different sizes of FG play distinct roles within the thermal conduction network: (1) large-scale FG (100 μm) provides efficient long-distance in-plane heat conduction pathways but easily forms large gaps, resulting in discontinuous conduction; (2) medium-scale FG (50 μm) acts as a bridging component, filling the gaps between larger flakes and enhancing network continuity; (3) small-scale FG (10 μm) further fills the smaller gaps between larger flakes, increasing the FG contact area and enhancing network compactness. Thus, the synergistic use of multi-scale FG effectively constructs an efficient thermal conduction network, particularly through increasing the proportion of small-scale FG (10 μm), thereby significantly improving the thermal performance of composites.

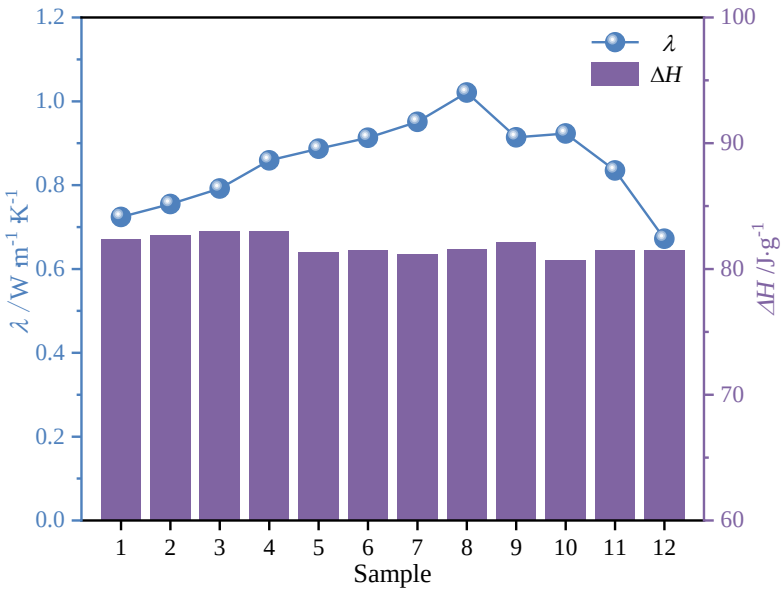

Figure 8. Thermal performance of composites with different FG size ratios.

To further reveal the influence of the FG mixing ratio on thermal conductivity and clarify the formation mechanism of FG-based thermal conduction networks, three representative volume element (RVE) models of multidimensional carbon-based microencapsulated phase change composites were constructed. The FG mixing ratios in these models were as follows: (a) 50% FG (10 μm) + 25% FG (50 μm) + 25% FG (100 μm); (b) 25% FG (10 μm) + 50% FG (50 μm) + 25% FG (100 μm); (c) 25% FG (10 μm) + 25% FG (50 μm) + 50% FG (100 μm). Finite element simulations of heat conduction were performed, and the resulting heat flux distributions and equivalent thermal conductivities are illustrated in Fig. 9. When the proportion of small-scale FG (10 μm) was higher, the thermal conduction pathways in the RVE model became more continuous and the heat flux distribution was more uniform, as shown in Fig. 9(a). This indicates higher efficiency in the thermal conduction network due to effective filling of gaps by small-scale FG, thereby increasing the contact area between FG flakes of different sizes. In this case, the equivalent thermal conductivity reached 0.908 W/(m K). Conversely, when the proportion of small-scale FG was lower, thermal conduction pathways showed noticeable discontinuity, significantly reducing thermal conduction efficiency, as shown by Figs. 9(b,c), with equivalent thermal conductivities dropping to 0.791 and 0.653 W/(m K), respectively. Thus, the synergistic effect of multi-scale FG is crucial for establishing efficient thermal conduction networks, and increasing the small-scale FG content is particularly essential for improving the overall thermal performance of phase change composites.

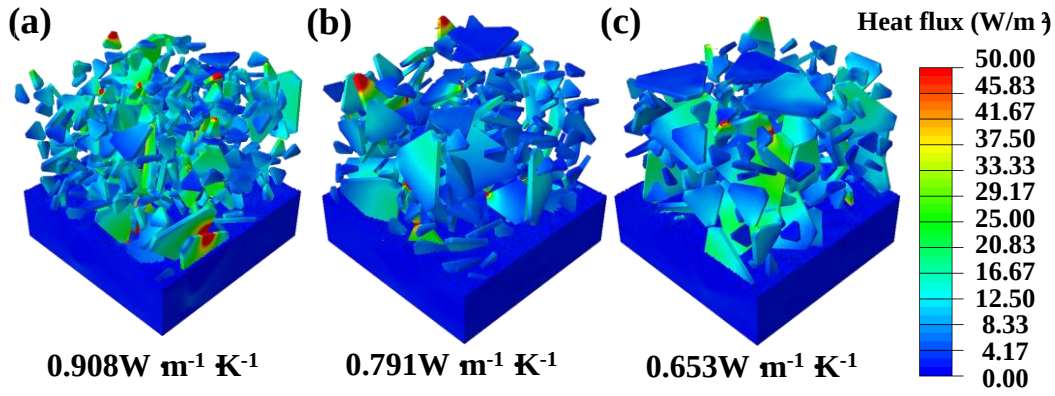

Figure 9. Heat flux distribution of RVE models with different FG size ratios.

3.5 Thermal cycling stability

To evaluate the thermal cycling stability of multidimensional carbon-based microencapsulated phase change composites, three representative samples (Samples 5, 8, and 10) were subjected to thermal cycling tests. Each cycle consisted of heating the sample to 80 ℃ for 10 min, followed by cooling to -10 ℃ for 10 min, and this process was repeated for up to 100 cycles. Fig. 10 presents the morphology and leakage characteristics of the three groups of composites under different thermal cycling conditions. After 100 thermal cycles, all samples retained their structural integrity without liquid leakage or notable deformation, indicating that the introduction of PCMC effectively prevents PCM leakage and enhances thermal cycling stability. To further investigate the effects of thermal cycling on thermal properties, λ and ΔH values of these composites at different cycle intervals were examined in Fig. 11. The results demonstrated that both λ and ΔH slightly decreased as the number of thermal cycles increased, but the magnitude of these changes was minor. These findings clearly demonstrate that the prepared multidimensional carbon-based microencapsulated phase change composites possess excellent stability and reliability under repeated thermal cycling conditions.

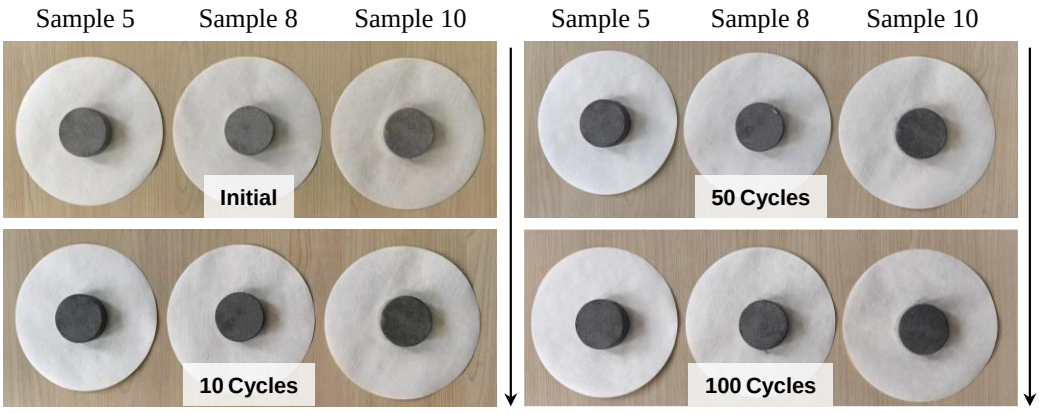

Figure 10. Morphology and leakage behavior of composites under thermal cycling.

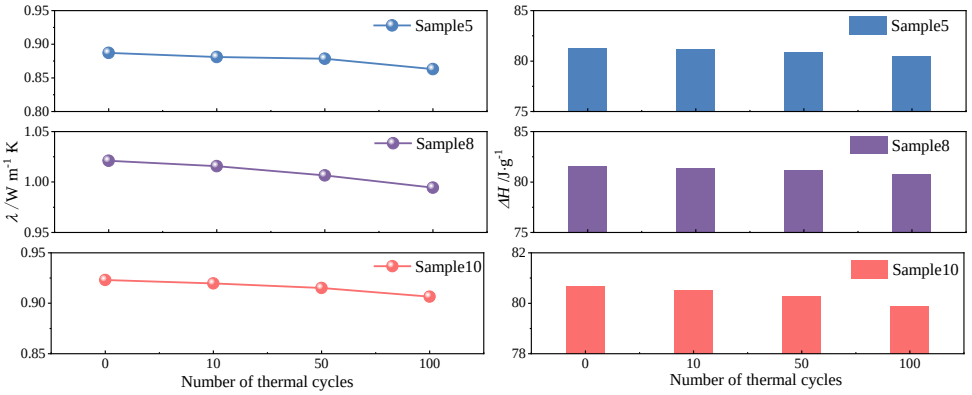

Figure 11. Thermal performance of phase change composites under different thermal cycling conditions: (a) λ and (b) ΔH.

4. Conclusion

In this study, multidimensional carbon-based microencapsulated phase change composites with enhanced thermal conductivity were successfully prepared using a hot-pressing method. The influences of various material components on the thermal properties of these composites were systematically studied by experimental tests combined with finite element simulations, and the formation mechanism of the multidimensional thermal conduction network within the composites was elucidated. The main conclusions are summarized as follows:

(1) The content of PCMC plays a critical role in balancing the composite's thermophysical properties. At an optimal PCMC content of 70%, a highly efficient multidimensional carbon-based thermal conduction network is formed, achieving an ideal balance between thermal conductivity and latent‑ heat capacity. In this case, the composite exhibits a high phase change enthalpy of 81.282 J/g.

(2) Multidimensional thermally conductive materials (PCF and FG) synergistically construct an enhanced carbon-based thermal conduction network. Specifically, the interwoven one-dimensional thermal pathways provided by PCF and two-dimensional channels formed by FG significantly enhance the composite's thermal conductivity. Compared with composites without PCF, the thermal conductivity increases by 153.4% while maintaining similar latent heat (81.282 J/g). Thus, the synergy between FG and PCF substantially shortens heat conduction paths, improves the thermal response, and provides strong support for thermal management during heat absorption and release cycles.

(3) Multi-scale FG composite filling significantly improves the connectivity and compactness of the thermal conduction network. By appropriately combining FGs of different scales, the thermal conductivity of the composite is effectively enhanced. Specifically,

large-scale FG provides long-distance conduction pathways; medium-scale FG fills larger voids and enhances connectivity; small-scale FG further fills smaller voids, increasing network compactness. With an optimized mixing ratio of 50% (10 μm), 33% (50 μm), and 17% (100 μm), the thermal conductivity of the composite reaches 1.021 W/(m·K), while maintaining a high latent heat of 81.540 J/g. Therefore, employing a multi-scale FG filling strategy, particularly increasing the proportion of small-scale FG, is crucial for constructing an efficient thermal conduction network.

References

[1] Li X Z, Tang G H, Wang Z H, Feng J C, Zhang X F 2024 Acta Phys. Sin. 73 184401

[2] Wang Z H, He C B, Hu Y, Tang G H 2024 Sci. China Tech. Sci. 67 2387

[3] Drissi S, Ling T C, Mo K H 2019 Thermochim Acta 673 198

[4] Wu W F, Liu N, Cheng W L, Liu Y 2013 Energy Convers. Manag. 69 174

[5] Kong Q Q, Jia H, Xie L J, Tao Z C, Yang X, Liu D, Sun G H, Guo Q G, Lu C X, Chen C M 2021 Compos. Part A 145 106391

[6] Velez C, Ortiz de Zarate J M, Khayet M 2015 Int. J. Therm. Sci. 94 139

[7] Haddad Z, Buonomo B, Abu-Nada E, Manca O 2024 Renew. Sustain. Energy Rev. 205 114826

[8] Chang Z, Wang K, Wu X H, Lei G, Wang Q, Liu H, Wang Y L, Zhang Q 2022 J. Energy Storage 46 103840

[9] Xu R, Xia X M, Wang W, Yu D 2020 Colloids Surf. A 591 124519

[10] Wang X T, Chen H X, Kuang D L, Huan X, Zeng Z Y, Qi C, Han S J, Li G Y 2024 Compos. Sci. Technol. 257 110836

[11] Zhang D F, Cai T Y, Li Y J, Li Y S, He F F, Chen Z G, Zhu L Q, He C D, Yang W B 2022 ChemistrySelect 7 e202202930

[12] Wu X H, Gao M T, Wang K, Wang Q W, Cheng C X, Zhu Y J, Zhang F F, Zhang Q 2021 J. Energy Storage 36 102398

[13] Lu X T, Qian R D, Xu X Y, Liu M, Liu Y F, Zou D Q 2024 Nano Energy 124 109520

[14] Tong Y L, Tao Z C, Li Y F, Liu Z J, Jiang L F, Yin Y Z 2022 Chinese Space Sci. Technol. 42 131

[15] Dubey A K, Sun J, Choudhary T, Dash M, Rakshit D, Ansari M Z, Ramakrishna S, Liu Y, Nanda H S 2023 Renew. Sustain. Energy Rev. 182 113421

[16] Li S Y, Yan T, Pan W G 2024 Cell Rep. Phys. Sci. 5 102046

[17] Xia Y P, Zhang H Z, Huang P R, Huang C W, Xu F, Zou Y J, Chu H L, Yan E H, Sun L X 2019 Chem. Eng. J. 362 909

[18] Nomura T, Tabuchi K, Zhu C, Sheng N, Wang S, Akiyama T 2015 Appl. Energy 154 678

[19] Cheng P, Chen X, Gao H Y, Zhang X W, Tang Z D, Li A, Wang G 2021 Nano Energy 85 105948

[20] Yang M S, Li X Y, Chen W Q 2024 Appl. Energy 371 123726

[21] Prieto R, Molina J M, Narciso J, Louis E 2011 Compos. Part A 42 1970

[22] Zhang H M, Chao M J, Zhang H S, Tang A, Ren B, He X B 2014 Appl. Therm. Eng. 73 739

[23] Tian W L, Qi L H, Chao X J, Liang J H, Fu M W 2019 Compos. Part B 162 1

[24] Xu J Z, Gao B Z, Du H D, Kang F Y 2016 Int. J. Therm. Sci. 104 348

[25] Xu J Z, Gao B Z, Kang F Y 2016 Appl. Therm. Eng. 102 972

[26] Zha J W, Wang F, Wan B Q 2025 Prog. Mater. Sci. 148 101362

[27] Yan X W, Xie Y, Fang Q Z, Hu Y, Xin Q Q 2024 Int. Commun. Heat Mass Transf. 159 108018

[28] Cernuschi F, Kulczyk-Malecka J, Zhang X, Nozahic F, Estournès C, Sloof W G 2023 J. Eur. Ceram. Soc. 43 6296